Joint Radio Frequency Interference and Deceptive Jamming Suppression Method for Single-Channel SAR via Subpulse Coding

Guoli Nie, Guisheng Liao, *Senior Member, IEEE*, Cao Zeng, *Member, IEEE*, Xuepan Zhang, and Dongchen Li

***Abstract*—The radio frequency interference (RFI) and deceptive jamming (DJ), as two major external threats to synthetic aperture radar (SAR) systems, can greatly reduce the readability and veracity of the obtained SAR images. Current interference suppression methods have no capability to suppress both of them. In this article, a subpulse coding (SPC)-based joint RFI and DJ suppression method for single-channel SAR systems is proposed. By making full use of the elaborate coding scheme and subpulse transmitting mode, SPC can effectively suppress RFIs in the Doppler domain. On the other hand, after the decoding process, by utilizing the subpulse digital beamforming (DBF) technology with the well-designed DBF weight vectors, DJs can also be suppressed greatly. Numerical experiments verify the effectiveness of the proposed method.**

***Index Terms*—Deceptive jamming (DJ), radio frequency interference (RFI), subpulse coding (SPC), synthetic aperture radar (SAR).**

NOMENCLATURE

RFI	Radio frequency interference.
DJ	Deceptive jamming.
SAR	Synthetic aperture radar.
DBF	Digital beamforming.
PRF	Pulse repetition frequency.
PRT	Pulse repetition time.
SJR	Signal-to-jamming ratio.
SNR	Signal-to-noise ratio.
RMSE	Root-mean-square-error.
SPC	Subpulse coding.
FNF	Frequency notch filtering.
IAA	Iterative adaptive approach.
SR	Sparse recovery.
RPC	Random phase coding.
AQPC	Azimuth quadratic phase coding.
NBI	Narrowband RFI.
LFM-WBI	Linear frequency modulation wideband RFI.
SM-WBI	Sinusoidal modulation wideband RFI.

Manuscript received 16 October 2022; revised 7 December 2022; accepted 20 December 2022. Date of publication 23 December 2022; date of current version 2 January 2023. This work was supported in part by the Innovative Research Group of the National Natural Science Foundation of China under Grant 61621005, in part by the National Natural Science Foundation of China under Grant 61771015, in part by the National Nature Science Foundation of China (NSFC) under Grant 62201408, and in part by the stabilization support of National Radar Signal Processing Laboratory under Grant JKW202108. *(Corresponding author: Cao Zeng.)*

Guoli Nie and Cao Zeng are with the National Laboratory of Radar Signal Processing, Xidian University, Xi'an 710071, China (e-mail: 20021110266@stu.xidian.edu.cn; czeng@mail.xidian.edu.cn).

Guisheng Liao and Xuepan Zhang are with the Hangzhou Institute of Technology, Xidian University, Hangzhou 311200, China, and also with the National Laboratory of Radar Signal Processing, Xidian University, Xi'an 710071, China (e-mail: liaogs@xidian.edu.cn; xpzhang7@163.com).

Dongchen Li is with the CSSC Systems Engineering Research Institute, Beijing 100094, China (e-mail: ldc19@mails.tsinghua.edu.cn).

Digital Object Identifier 10.1109/JSTARS.2022.3231606

I. INTRODUCTION

SAR, breaking through limitations of the traditional optical remote sensing system that is time constrained and cannot effectively obtain the information of the detection scene in harsh natural environments, has received widespread attention and become an indispensable technology in remote sensing systems. However, owing to its unique imaging mechanism, SAR is especially vulnerable to interferences emitted by external sources during work. Although the SAR system itself has a 2-D matching filter that can reduce the impact of some interferences, interferences can also greatly reduce the image quality of SAR when energies of them are high, or they have a good correlation with the matching filter.

Among the many interferences, the RFI and DJ are the most threatening to the SAR system. Owing to the limited spectrum resources and the requirement for SAR to transmit large bandwidth signals to achieve high resolution in range, a large number of high-energy signals (collectively referred to as RFIs) emitted by base stations, such as mobile phones and broadcasters, enter the frequency band occupied by SAR signals [1], [2], [3], [4]. Eventually, RFIs appear in the SAR image as extremely bright line segments. These bright lines will block ground-scattering targets and hinder the acquisition of scene information from the SAR system. The DJ is quite different from the RFI. The jammer intercepts SAR signals, modulates the delays and amplitudes of them to form jammings that are coherently related to the SAR matching filter, and then retransmits them. Therefore, in the final SAR image, DJs will form very deceptive false patches, which will affect the judgment of the SAR system regarding the ground information severely [5].

In recent years, scholars have gradually paid attention to the harms caused by these interferences. Therefore, interference suppression technology for SAR is now becoming a hot research spot [6], [7], [8]. In terms of RFI suppression methods, they

can be roughly divided into three categories: nonparametric [9], [10], [11], parametric [12], [13], [14], [15], and semiparametric [16], [17], [18], [19], [20], [21], [22], [23]. Among them, nonparametric methods normally focus on the setting of notching filters in the frequency domain, which can greatly suppress RFIs. However, SAR signals located in notches of filters are also filtered, which will affect the SAR image. This impact is especially evident when RFIs are wideband. Although a removed spectrum IAA is proposed in [11] to recover the damaged SAR signal spectrum, even so, when bandwidths of RFIs are relatively large, SAR signals are still difficult to be recovered perfectly. The common basic idea of parameter methods is the subspace projection. That is, we try to find RFIs corresponded subspaces and project the original polluted data to the complement of RFI subspaces to obtain the cleaned SAR signals. Similarly, when RFIs are wideband, they occupy a considerable amount of subspaces, that is, a large number of SAR signals locate in the same subspaces as the RFIs. These SAR signals will also be canceled. In [13], an IAA method is proposed to suppress RFIs by projection in each time slice after converting wideband RFIs (WBIs) into narrowband in the time–frequency domain by short-time Fourier transform, which greatly reduces the loss of SAR signal. Nevertheless, still, some SAR signals are inevitably lost. On the other hand, with the development of SR technologies, many scholars have successfully used them in RFI suppression. We call these semiparametric methods. Note that most of them are used in NBI suppression because NBIs own the sparse property in the frequency domain, while WBIs do not. In [22], an SR-based WBI suppression method is proposed by noting that WBIs are sparse in the time–frequency domain. Generally speaking, SR methods can suppress RFI as much as possible on the basis of protecting SAR signals by accurately selecting regularization parameters. However, these regularization parameters are always hard to be optimal; furthermore, in the process of protecting SARs, some RFIs with low energies remain.

In terms of DJ suppression, methods can be roughly divided into two categories: fixed waveform methods [24], [25], [26], [27] and agile waveform methods [28], [29]. For the fixed waveform methods, they can suppress intrapulse DJs, and the system complexities of them are always very low. However, they are only suitable for sparse scenarios; moreover, they are failed to suppress DJs having the same zero-Doppler moments as intercepted SAR signals [27]. Agile waveform methods normally encode the transmitted signals pulse by pulse. A necessary assumption is that jammers need at least one PRT to generate jammings. This is reasonable since jammers do need time to obtain the information of the SAR system to modulate intercepted signals. Therefore, in this case, DJs and SAR signals in the same echo pulse will have differences in phase information. These differences can be well reflected in the Doppler domain. Thus, by setting up proper filters in the Doppler domain, DJs can be filtered out very well.

As the matter of fact, all the above algorithms can only suppress a certain kind of interference (RFI or DJ). Therefore, it is undoubtedly a huge advance if an algorithm can suppress multiple kinds of interferences. In this article, a joint RFI and DJ suppression algorithm based on SPC for the single-channel SAR system is proposed. By cleverly designing the coding elements and encoding subpulses, the proposed method can effectively separate RFIs and SAR signals; on the other hand, after completing the RFI suppression and decoding procedure, DJs can also be greatly suppressed by the subpulse DBF technology. In this article, we also design two DBF weight vectors and analyze the DJ suppression performance under each of them. It is demonstrated that the proposed SPC approach can suppress both RFIs and DJs by numerical experiments.

The rest of this article is organized as follows. In Section II, we briefly make an introduction about RFI and DJ signal models, respectively. The proposed method is introduced in Section III. In Section IV, numerical experiments as well as analyses are conducted. Finally, Section V concludes this article. To enhance the readability of this article for readers, main abbreviations are listed in the Nomenclature.

II. Signal Models of RFI and DJ

A. RFI Signal Model

The total signal of SAR for any single pulse with RFIs can be modeled as

$$y(t) = s(t) + r(t) + n(t) \tag{1}$$

where $y(t)$ is the total signal in this echo pulse. $s(t)$ and $n(t)$ stand for SAR signals and Gaussian white noises, respectively. $r(t)$ is for the sum of RFIs. When considering NBIs, $r(t)$ can be formulated as the sum of I complex sinusoidal signals

$$r_{\text{NBI}}(t) = \sum_{i=1}^{I} A_i e^{j2\pi f_i t} \tag{2}$$

where I is the number of NBIs and each of them is with frequency f_i and complex amplitude A_i. t is the fast time. $j = \sqrt{-1}$.

On the other hand, if WBIs are in consideration, then $r(t)$ can be modeled as the sum of linear frequency modulation (LFM) signals or the sum of sinusoidal modulation (SM) signals [1]. That is, for LFM-WBI signals, we have

$$r_{\text{LFM}}(t) = \sum_{i=1}^{I} A_i e^{j2\pi(f_i t + \frac{1}{2}\gamma_i t^2)} \tag{3}$$

where A_i, f_i, and γ_i are the complex amplitude, frequency, and chirp rate for the ith LFM-WBI component, respectively.

Similarly, for the SM-WBI, we have

$$r_{\text{SM}}(t) = \sum_{i=1}^{I} A_i e^{j\beta_i \sin(2\pi f_i t + \phi_i)} \tag{4}$$

where A_i, f_i, β_i, and ϕ_i are the complex amplitude, frequency, modulation coefficient, and initial phase for the ith SM-WBI component, respectively.

By comparing (2) and (3), one can easily find that NBI can be seen as a special case of LFM-WBI with chirp rate $\gamma_i = 0$. Thus, in the rest of this article, we only consider LFM-WBI and SM-WBI signals.

The frequency spectrum of LFM-WBI- and SM-WBI-contained SAR signals for a pulse is shown in Fig. 1(a). We see clearly that both LFM-WBI and SM-WBI occupy a certain

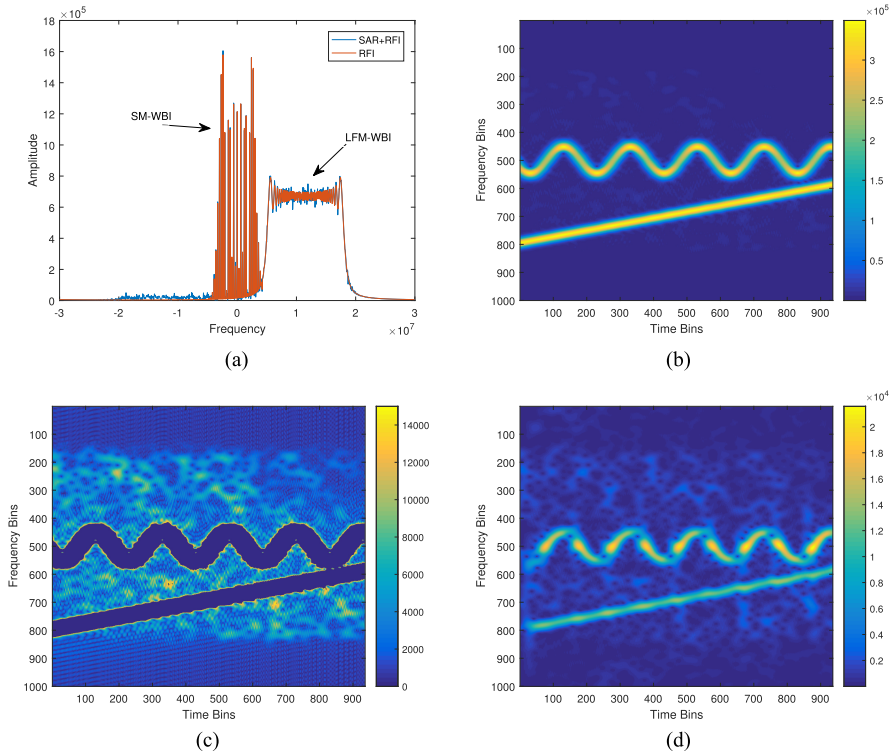

Fig. 1. Energy distributions of RFIs. (a) In the frequency domain before suppressing. (b) In the time–frequency domain before suppressing. (c) In the time–frequency domain after suppressing by parametric methods. (d) In the time–frequency domain after suppressing by semiparametric methods.

bandwidth. That is, energies of them cannot well concentrate in the frequency domain, or say, they are nonsparse. Therefore, it is quite difficult to suppress WBIs as well as to protect SAR signals at the same time in the frequency domain. Fig. 1(b) shows the energy distribution of WBIs in the time–frequency plane. Apparently, they own the sparse property. The RFI suppression results of parametric and semiparametric methods for a SAR pulse are shown in Fig. 1(c) and (d), respectively. Obviously, in Fig. 1(c), one can see that two notches appear in the positions of RFIs, while SAR signals in these places are also suppressed inevitably. From Fig. 1(d), one can see that for the semiparametric method, although RFIs are greatly suppressed while SAR signals are well protected, still, some RFI energies exist.

B. DJ Signal Model

Signal transmitted by SAR at the slow-time moment t_a is

$$s\left(t,t_a\right)=w_r(t)w_a\left(t_a\right)\exp\left(j2\pi f_c t\right)\exp\left(j\pi\gamma t^2\right) \quad (5)$$

where $w_r(t)$ and $w_a(t)$ are range and azimuth window functions, respectively. f_c is the carrier frequency and γ is the chirp rate. The intercepted signal by the jammer at J is

$$s_{J\_int}\left(t,t_a\right)=s\left(t,t_a\right)\otimes\delta\left(t-\frac{R_J\left(t_a\right)}{c}\right)$$
$$=w_r\left(t-\frac{R_J\left(t_a\right)}{c}\right)w_a\left(t_a\right)$$
$$\exp\left(j2\pi f_c\left(t-\frac{R_J\left(t_a\right)}{c}\right)\right)$$
$$\exp\left(j\pi\gamma\left(t-\frac{R_J\left(t_a\right)}{c}\right)^2\right) \quad (6)$$

where $R_J(t_a)$ is the instant slant from the radar platform to the jammer at this moment, $\otimes$ is the convolution operator, δ is the Dirac delta function, and c is the velocity of light.

After intercepting the SAR signal, the jammer modulates it as follows:

$$s_{J\_\mathrm{mod}}\left(t,t_a\right)=\sigma_P s_{J\_\mathrm{int}}\left(t,t_a\right)$$
$$\otimes\delta\left(t-\frac{2R_P\left(t_a-\tau\right)}{c}+\frac{2R_J\left(t_a\right)}{c}\right) \quad (7)$$

where $R_P(t_a-\tau)$ is the instant slant from the radar platform to another point P, σ_P is the scattering coefficient at P, and τ is the zero-Doppler moment for P.

Therefore, after being retransmitted by the jammer, the DJ received by the radar is

$$s_J\left(t,t_a\right)=s_{J\_\mathrm{mod}}\left(t,t_a\right)\otimes\delta\left(t-\frac{R_J\left(t_a\right)}{c}\right)$$
$$=\sigma_P w_r\left(t-\frac{2R_P\left(t_a-\tau\right)}{c}\right)w_a\left(t_a\right)$$
$$\exp\left(j2\pi\left(t-\frac{2R_P\left(t_a-\tau\right)}{c}\right)\right)$$
$$\exp\left(j\pi\gamma\left(t-\frac{2R_P\left(t_a-\tau\right)}{c}\right)^2\right) \quad (8)$$

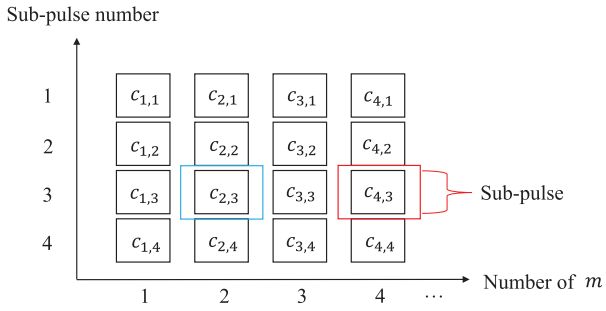

Fig. 2. Diagram for the proposed coding strategy.

while the true echo from P is

$$s_P(t,t_a) = \sigma_P w_r\left(t-\frac{2R_P(t_a-\tau)}{c}\right) w_a(t_a-\tau) \exp\left(j2\pi\left(t-\frac{2R_P(t_a-\tau)}{c}\right)\right) \exp\left(j\pi\gamma\left(t-\frac{2R_P(t_a-\tau)}{c}\right)^2\right). \quad (9)$$

We see from (8) that the DJ has great coherence with the SAR system; on the other hand, the only difference between (8) and (9) is the Doppler support area or the zero-Doppler moment, which is reflected in the azimuth window function. This is the key for fixed-waveform-based methods to suppress DJs. Nevertheless, in the case of $\tau = 0$, i.e., DJs and SAR signals have the same Doppler support areas, (8) and (9) are the same. Thus, these methods are not effective anymore.

III. Proposed Method

In this section, we will formally introduce the proposed method. The coded subpulse model and the signal processing procedure for SAR imaging are first discussed. Principles of RFI and DJ suppression, as well as the designed DBF weight vectors, are subsequently introduced.

A. Signal Model and Processing Procedure

1) Transmitted Subpulse Model: At any slow-time moment, SAR transmits K subpulses. Specifically, the expression of the kth subpulse at the mth slow-time moment t_m is

$$s_{m,k}(t,t_m) = \text{rect}\left(\frac{t}{T_{sp}}\right)\exp(j2\pi f_c t)\exp\left(j\pi\gamma t^2\right) \otimes \delta(t-(k-1)\Delta t)\cdot c_{m,k} \quad (10)$$

where T_{sp} is the subpulsewidth, Δt is the time delay between two adjacent subpulses, and $c_{m,k}$ is the coding term, which is designed as

$$c_{m,k} = \exp\left(j2\pi\frac{(m-1)k}{K+1}\right), \quad k = 1,2,\ldots,K. \quad (11)$$

The whole coding strategy is shown explicitly in Fig. 2, where $K = 4$. For instance, when $m = 2$ and $k = 3$, the expression of the corresponding subpulse (the blue rectangle) is

$$s_{2,3}(t,t_m) = \text{rect}\left(\frac{t}{T_{sp}}\right)\exp(j2\pi f_c t)\exp\left(j\pi\gamma t^2\right) \otimes \delta(t-2\Delta t)\exp\left(j2\pi\frac{1\cdot 3}{5}\right). \quad (12)$$

2) Separation of Echo Signals: Since the transmitting interval between two adjacent subpulses is extremely short, all the corresponding subpulse echos will be overlapped. Here, we separate them in the Doppler domain by using the designed coding terms.

Considering the mth slow-time moment t_m and a true ground target P, the first subpulse echo is

$$s_{m,1}(t,t_m) = \text{rect}\left(\frac{t-\frac{2R_p(t_m)}{c}}{T_{sp}}\right)\exp\left(j2\pi\frac{(m-1)\cdot 1}{K+1}\right) \exp\left(j2\pi f_c\left(t-\frac{2R_p(t_m)}{c}\right)\right)\exp\left(j\pi\gamma\left(t-\frac{2R_p(t_m)}{c}\right)^2\right). \quad (13)$$

Moreover, we have

$$R_p(t_m) \approx R_{p0} + \frac{v^2 t_m^2}{2R_{p0}} \quad (14)$$

and

$$m-1 = f_{\text{PRF}}\cdot t_m \quad (15)$$

where R_{p0} is the shortest slant from radar to P, f_{PRF} is the PRF, and v is the velocity of the radar platform.

Therefore, by combining (13)–(15), we see that the Doppler history of P at this subpulse in a synthetic aperture time is

$$f_{\text{Doppler1}} = \gamma_P t_m + \frac{f_{\text{PRF}}}{K+1}, \quad t_m \in \left[-\frac{T_a}{2},\frac{T_a}{2}\right] \quad (16)$$

where T_a is the synthetic aperture time and $\gamma_P = -\frac{2v^2}{\lambda R_{P0}}$ is the Doppler chirp rate. λ is the wavelength.

In the same way, we can also know that the Doppler history of P at the second subpulse is

$$f_{\text{Doppler2}} = \gamma_P t_m + \frac{2f_{\text{PRF}}}{K+1}, \quad t_m \in \left[-\frac{T_a}{2},\frac{T_a}{2}\right]. \quad (17)$$

Therefore, from (16) and (17), we conclude that the overlapped echos can be separated by Doppler filters as long as the following condition is satisfied:

$$f_{\text{PRF}} > (K+1)\cdot B_d \quad (18)$$

where $B_d = \gamma_P T_a$ is the Doppler bandwidth.

Distributions of energies of coded subpulses in the range–Doppler domain are shown in Fig. 3(a). The slice of Fig. 3(a) is shown in Fig. 3(b).

As the matter of fact, we see that through coding, Doppler centers of subpulses are shifted. When shifts are big enough, Doppler histories of subpulse echos are becoming mutually disjoint. At this time, it is convenient for us to separate them in the Doppler domain.

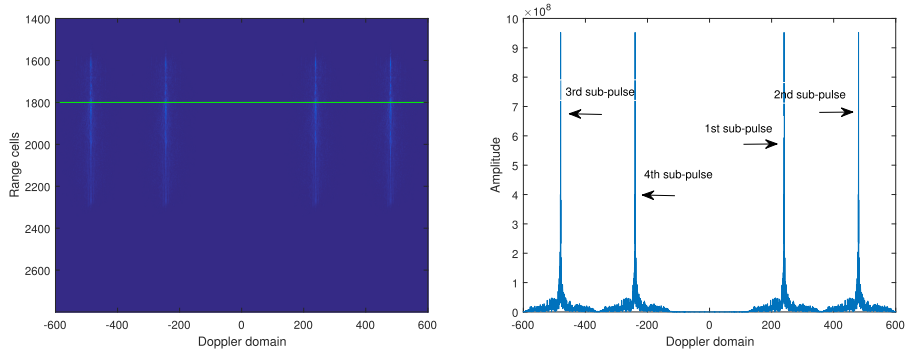

Fig. 3. Distributions of energies of subpulses. (a) In the range–Doppler domain. (b) Slice of (a) at range cell 1800.

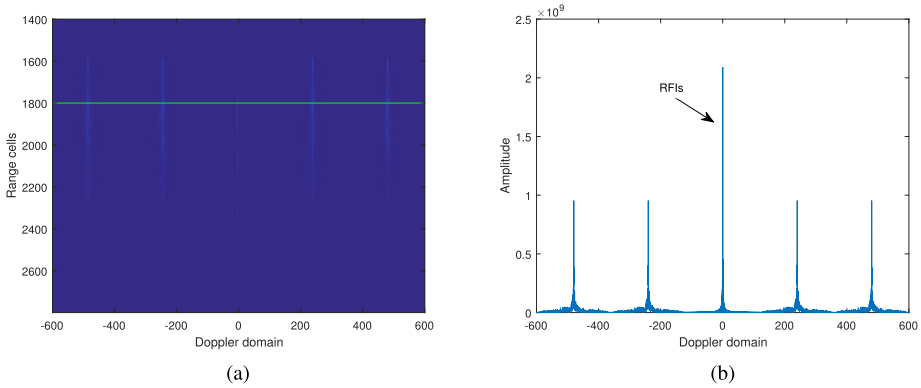

Fig. 4. Distributions of energies of subpulses and RFIs. (a) In the range–Doppler domain. (b) Slice of (a) at range cell 1800.

3) Subpulse Slow-Time Decoding and Fast-Time Aligning: Now, we have obtained K coded subpulses after the above separation procedure. At this time, we decode and align each subpulse as follows:

$$s_{m,k}\left(t,t_m\right)=s_{m,k}\left(t,t_m\right)\cdot c_{m,k}^{*}\otimes\delta\left(t+\left(k-1\right)\Delta t\right) \quad (19)$$

where $*$ is the conjugate operator. Now, all subpulses at t_m have the same expression

$$s_{m,k}\left(t,t_m\right)= \operatorname{rect}\left(\frac{t-\frac{2R_p(t_m)}{c}}{T_{sp}}\right)\exp\left(j2\pi f_c\left(t-\frac{2R_p\left(t_m\right)}{c}\right)\right) \exp\left(j\pi\gamma\left(t-\frac{2R_p\left(t_m\right)}{c}\right)^2\right). \quad (20)$$

B. Principle of RFI Suppression

Denote $r(t)$ as the sum of RFIs. Note the fact that 1) RFIs do not participate in the coding procedure and 2) the Doppler support area for $r(t)$ is $[-\frac{T_a}{2},\frac{T_a}{2}]$. The first fact is because RFIs are external signals, while the second fact is based on that RFIs are always considered to be received by SAR at the main lobe. Therefore, under the condition of inequality (18) and before the decoding procedure, energies of RFIs are concentrated in the range of $[-\frac{f_{\text{PRF}}}{2(K+1)},\frac{f_{\text{PRF}}}{2(K+1)}]$ in the Doppler domain, in which no SAR signals locate, as shown in Fig. 4. The total RFI here consists of one LFM-WBI and one SM-WBI, with both energies of 60 dB. From Fig. 4, one can see that RFIs and SAR signals are separated. Therefore, we can easily suppress RFIs in the Doppler domain by filtering. As the matter of fact, there is no need for us to set the extra Doppler filter to filter out RFIs since we have equivalently suppressed them when separating subpulse echos.

C. Principle of DJ Suppression

Suppose that the modulation time of the jammer is $n\cdot t_{\text{PRT}}(n\in N^{+},\operatorname{mod}(n,K+1)\neq 0)$, where t_{PRT} is the PRT. Consider that the mth full-pulse is intercepted by the jammer. After modulation and retransmission, DJs, as well as the $(m+n)$th subpulse echos, are received by SAR. Denote DJs as d_m. Thus, the kth subpulse of d_m is

$$d_{m,k}(t)=\operatorname{rect}\left(\frac{t-\frac{2R_p(t_m)}{c}}{T_{sp}}\right) \exp\left(j\pi\gamma\left(t-\frac{2R_p\left(t_m\right)}{c}\right)^2\right)$$

$$\exp\left(j2\pi f_c\left(t-\frac{2R_p\left(t_m\right)}{c}\right)\right)$$
$$\exp\left(j2\pi\frac{(m-1)\,k}{K+1}\right)\otimes\delta\left(t-(k-1)\,\Delta t\right) \tag{21}$$

while the true echos of kth subpulse for SAR are

$$s_{m+n,k}(t)=\text{rect}\left(\frac{t-\frac{2R_p(t_{m+n})}{c}}{T_{sp}}\right)$$
$$\exp\left(j\pi\gamma\left(t-\frac{2R_p\left(t_{m+n}\right)}{c}\right)^2\right)$$
$$\exp\left(j2\pi f_c\left(t-\frac{2R_p\left(t_{m+n}\right)}{c}\right)\right)$$
$$\exp\left(j2\pi\frac{(m+n-1)\,k}{K+1}\right)\otimes\delta\left(t-(k-1)\,\Delta t\right). \tag{22}$$

Therefore, after slow-time decoding and fast-time aligning, (21) turns into

$$\begin{aligned}d_{m,k}(t)&=d_{m,k}(t)\cdot c^*_{m+n,k}\otimes\delta\left(t+(k-1)\,\Delta t\right)\\&=\text{rect}\left(\frac{t-\frac{2R_p(t_m)}{c}}{T_{sp}}\right)\\&\exp\left(j\pi\gamma\left(t-\frac{2R_p\left(t_m\right)}{c}\right)^2\right)\\&\exp\left(j2\pi f_c\left(t-\frac{2R_p\left(t_m\right)}{c}\right)\right)\exp\left(-j2\pi\frac{nk}{K+1}\right)\\&=g_m(t)\exp\left(-j2\pi\frac{nk}{K+1}\right)\end{aligned} \tag{23}$$

while (22) turns into

$$s_{m+n,k}(t)=\text{rect}\left(\frac{t-\frac{2R_p(t_{m+n})}{c}}{T_{sp}}\right)$$
$$\exp\left(j\pi\gamma\left(t-\frac{2R_p\left(t_{m+n}\right)}{c}\right)^2\right)$$
$$\exp\left(j2\pi f_c\left(t-\frac{2R_p\left(t_{m+n}\right)}{c}\right)\right). \tag{24}$$

Thus, by comparing (23) and (24), we see that an extra coding term appears in (23). Next, we will make use of the subpulse DBF technology for DJ suppression. Denote the DBF weight vector as $\boldsymbol{w}$. We can let $\boldsymbol{w}$ be an all one vector with length K. That is, we have

$$\boldsymbol{w}=[1,1,\ldots,1]^T_{K\times1}. \tag{25}$$

Therefore, after DBF, the total signal $x_{m+n}(t)$ can be expressed as follows:

$$\begin{aligned}x_{m+n}(t)&=Ks_{m+n,k}(t)+\sum_{k=1}^{K}d_{m,k}(t)\\&=Ks_{m+n,k}(t)+g_m(t)\sum_{k=1}^{K}\exp\left(-j2\pi\frac{nk}{K+1}\right).\end{aligned} \tag{26}$$

Note that

$$\sum_{k=0}^{K}\exp\left(-j2\pi\frac{nk}{K+1}\right)=0$$
$$\Rightarrow\sum_{k=1}^{K}\exp\left(-j2\pi\frac{nk}{K+1}\right)=-1. \tag{27}$$

Then, (26) turns into

$$x_{m+n}(t)=Ks_{m+n,k}(t)-g_m(t). \tag{28}$$

We see that after subpulse DBF with the all one weight vector (next we denote it as DBF1), true SAR signals can achieve coherent superposition, while DJ signals cannot. The DBF1 pattern is shown in Fig. 5(a). Here, $K=4$. From Fig. 5(a) or (27), we see that no matter what n is (as long as under the condition $[n\in N^+,\text{mod}(n,K+1)\neq0)]$, amplitudes of DJ corresponded beams are always 1, while true SAR signals corresponded beam is K. The SJR can be improved by $20\log_{10}K(\text{dB})$. Therefore, this DBF1 strategy can enhance SJR effectively, which is equivalent to suppress DJs.

Nevertheless, in some cases, for example, when false scenes locate in small radar cross-section backgrounds like rivers, the above DJ suppression performance may still not be enough. Thus, here, we design another DBF (next we denote it as DBF2) weight vector to achieve a greater DJ suppression performance. First of all, we need to make a digital beam scan on subpulses to obtain n. This is quite easy since we can achieve n according to the peak positions of the DBF scan pattern.

Denote the kth element in the DBF2 weight vector $\boldsymbol{w}$ as $w(k)$. Jammings after DBF2 can be expressed as

$$d_m(t)=g_m(t)\sum_{k=1}^{K}\left[w^*(k)\exp\left(-j2\pi\frac{nk}{K+1}\right)\right]. \tag{29}$$

Design $w(k)$ as

$$w(k)=\begin{cases}\exp\left(j2\pi\frac{kn}{K(K+1)}\right), & \text{mod}(n,K+1)\leq\frac{K}{2}\\ \exp\left(j2\pi\frac{k(n-(K+1))}{K(K+1)}\right), & \text{mod}(n,K+1)>\frac{K}{2}\end{cases}. \tag{30}$$

Therefore, when $\text{mod}(n,K+1)\leq\frac{K}{2}$, (29) turns into

$$\begin{aligned}d_m(t)&=g_m(t)\cdot\\&\sum_{k=1}^{K}\left[\exp\left(-j2\pi n\frac{k}{K\left(K+1\right)}\right)\exp\left(-j2\pi n\frac{k}{K+1}\right)\right]\\&=g_m(t)\sum_{k=1}^{K}\exp\left(-j2\pi n\frac{k}{K}\right)\\&=0\end{aligned} \tag{31}$$

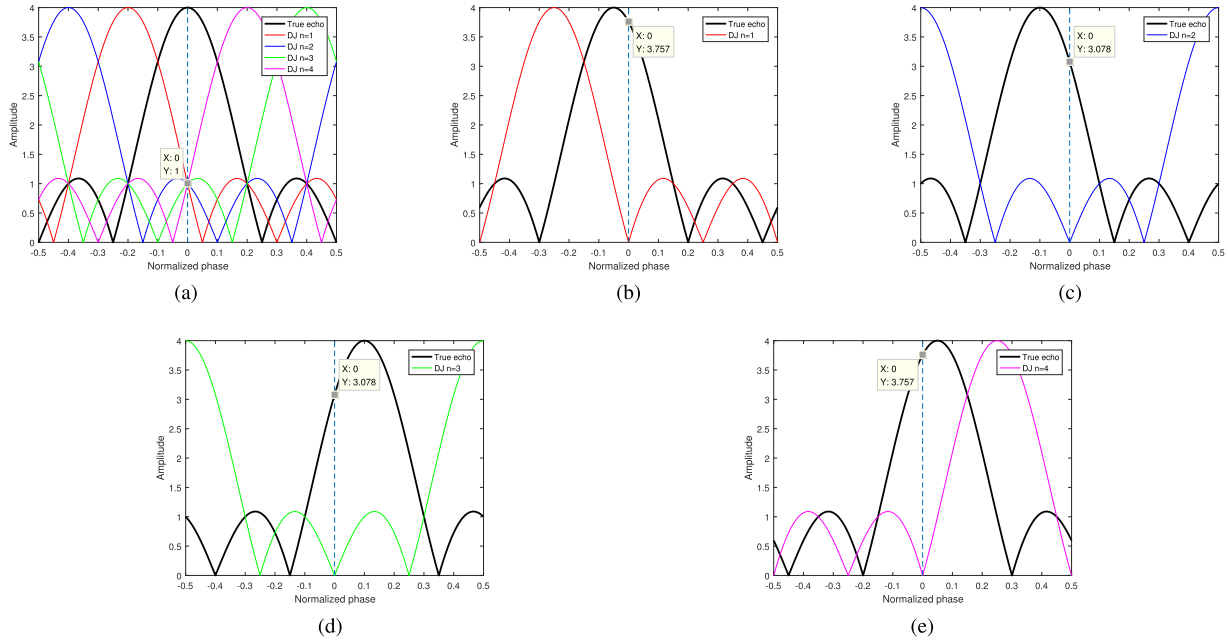

Fig. 5. DBF patterns. (a) DBF1. (b) DBF2: $n = 1$. (c) DBF2: $n = 2$. (d) DBF2: $n = 3$. (e) DBF2: $n = 4$.

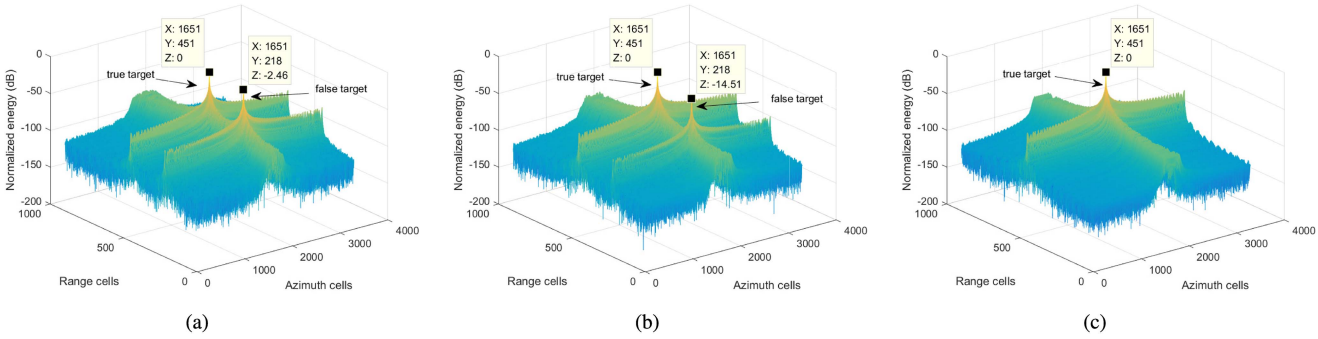

Fig. 6. Point target image. (a) Without DJ suppression. (b) DJ suppression by DBF1. (c) DJ suppression by DBF2.

while when $\mathrm{mod}(n, K+1) > \frac{K}{2}$, (29) turns into

$$d_m(t) = g_m(t) \cdot \sum_{k=1}^{K} \left[\exp\left(-j2\pi \frac{k\,(n-(K+1))}{K\,(K+1)} \right) \exp\left(-j2\pi n \frac{k}{K+1} \right) \right]$$

$$= g_m(t) \cdot \sum_{k=1}^{K} \left[\exp\left(j2\pi \frac{k\,(1-n)}{K} \right) \right]$$

$$= 0. \tag{32}$$

The DBF2 patterns under different n are shown in Fig. 5(b)–(e). One can see that although SAR signals from each subpulse cannot achieve coherence superposition, DJs are greatly suppressed. To see the suppression performance more intuitively, we conduct a brief point target numerical experiment. The results are shown in Fig. 6. From Fig. 6(a) and (b), one can see that the energy of the false target is suppressed by 12.05 dB after DBF1, while in Fig. 6(c), the false target is disappeared after DBF2.

At this time, we have accomplished the task of suppressing RFIs and DJs and obtained the cleaned SAR data. The whole process procedure is summarized in Fig. 7.

Remark: In this article, we only discuss one deceptive jammer with a fixed demodulation time. In the case that there are multiple jammers or DJs that have different demodulation times n, only the DBF1 technology can be used successfully.

D. Analyses of Subpulse Number K

The subpulse number K plays an important role in the proposed method since it is related to many SAR system parameters. Therefore, in this subsection, we make a discussion about K.

1) Unambiguous Range and Range Resolution: From the inequality (18), we know that a large f_{PRF} is necessary for the proposed method. A large f_{PRF} may, however, result in

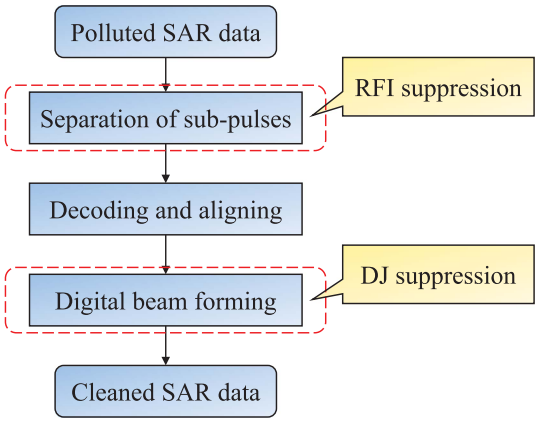

Fig. 7. Flowchart for the proposed method.

the range ambiguous. Specifically, the unambiguous range R_u should satisfy

$$R_u \leq \frac{c}{2f_{\text{PRF}}}. \tag{33}$$

replacing the inequality (18) into it yields

$$R_u \leq \frac{c}{2\left(K+1\right)B_a}. \tag{34}$$

Therefore, one can see that as K increases, the maximum unambiguous range decreases.

On the other hand, the width of each range cell of the subpulse system is

$$\Delta R_r = \frac{cK}{2B_r} \tag{35}$$

where $B_r = \gamma T_p$ and T_p is the full-pulsewidth. Thus, as K increases, the range resolution also decreases.

2) Probability of DJ Suppression: Recall the extra phase term in (23), i.e.,

$$\exp\left(-j2\pi\frac{nk}{K+1}\right). \tag{36}$$

When $\text{mod}(n, K+1) = 0$ is satisfied, its value is 1. Thus, at this time, DJs and SAR signals are indistinguishable. Practically, we have no information about the modulation time of the jammer when designing system parameters of SAR. Therefore, the probability of $\text{mod}(n, K+1) \neq 0$ is

$$P_K = \frac{K}{K+1} = 1 - \frac{1}{K+1} \tag{37}$$

which is also the probability of successfully suppressing DJs. One can see that with the increase of K, P_K is getting higher.

In summary, under the precondition of satisfying requirements of the SAR system and SAR image quality, K should be chosen relatively large.

IV. Numerical Experiments

In this section, some numerical experiments are conducted, as well as performance analyses are made. Note that the amplitude quantization range for each SAR image in this section is $[0, \sqrt{P_{\max}}]$, in which $P_{\max}$ is the maximal pixel value in each SAR image. Main parameters of the SAR system are shown in Table I.

TABLE I
Main Parameters of the SAR System

Parameters	Values
Carrier frequency	9.6 GHz
PRF	1200 Hz
Sampling frequency	70 MHz
Subpulse bandwidth	45 MHz
Subpulse number	4
Subpulse duration	1×10^{-5}s
Velocity	100 m/s
Radar azimuthal aperture	1 m

TABLE II
Quantitative Results of RFI Suppression

Method	RMSE	SNR (dB)
FNF	55.5607	−0.1951
IAA	44.0584	1.8197
SR	19.5108	8.8916
SPC	8.0258	16.5493

A. RFI Suppression Performance Analyses

In this subsection, we focus on investigating the RFI suppression performance of the proposed method. The total RFIs conclude one LFM-WBI and one SM-WBI, both of which are energies of 60 dB. Here, we choose some representative RFI suppression methods (FNF [10], IAA [13], and SR [22]) as comparisons. Experimental results are shown in Fig. 8.

From Fig. 8(a) and (b), we can see that under the impact of RFIs, information on ground scatters is covered by bright lines. Qualitatively, we see in Fig. 8(c) and (d) that although RFIs are almost suppressed (bright lines are almost disappeared), qualities of final SAR images are still not satisfactory since features of ground targets are also disappeared. On the contrary, in Fig. 8(e) and (f), not only RFIs are successfully suppressed, but also SAR echos are well protected. To make further comparisons and analyses of these methods, we conduct a quantitative experiment based on RMSE and SNR indices [30]

$$\text{RMSE}\left(\boldsymbol{Q}, \widehat{\boldsymbol{Q}}\right) = \frac{1}{Nr \times Na}\left\|\boldsymbol{Q} - \widehat{\boldsymbol{Q}}\right\|_F \tag{38}$$

$$\text{SNR}\left(\boldsymbol{Q}, \widehat{\boldsymbol{Q}}\right) = 20\log_{10}\frac{\text{RMSE}\left(\boldsymbol{Q}\right)}{\text{RMSE}\left(\boldsymbol{Q}, \widehat{\boldsymbol{Q}}\right)} \tag{39}$$

where $\boldsymbol{Q}$ and $\widehat{\boldsymbol{Q}}$ are SAR data matrix without RFIs and SAR data matrix after RFI suppression, respectively. $\|\cdot\|_F$ is the Frobenius norm. N_r and N_a are the number of rows and columns of $\boldsymbol{Q}$, respectively. Quantitative results are shown in Table II.

Now, we make analyses about the experiment results. For the FNF method, as we discussed before, when filtering out RFIs, SAR signals in the same frequency band of RFIs are also suppressed. In this WBI case, it causes huge damage to the

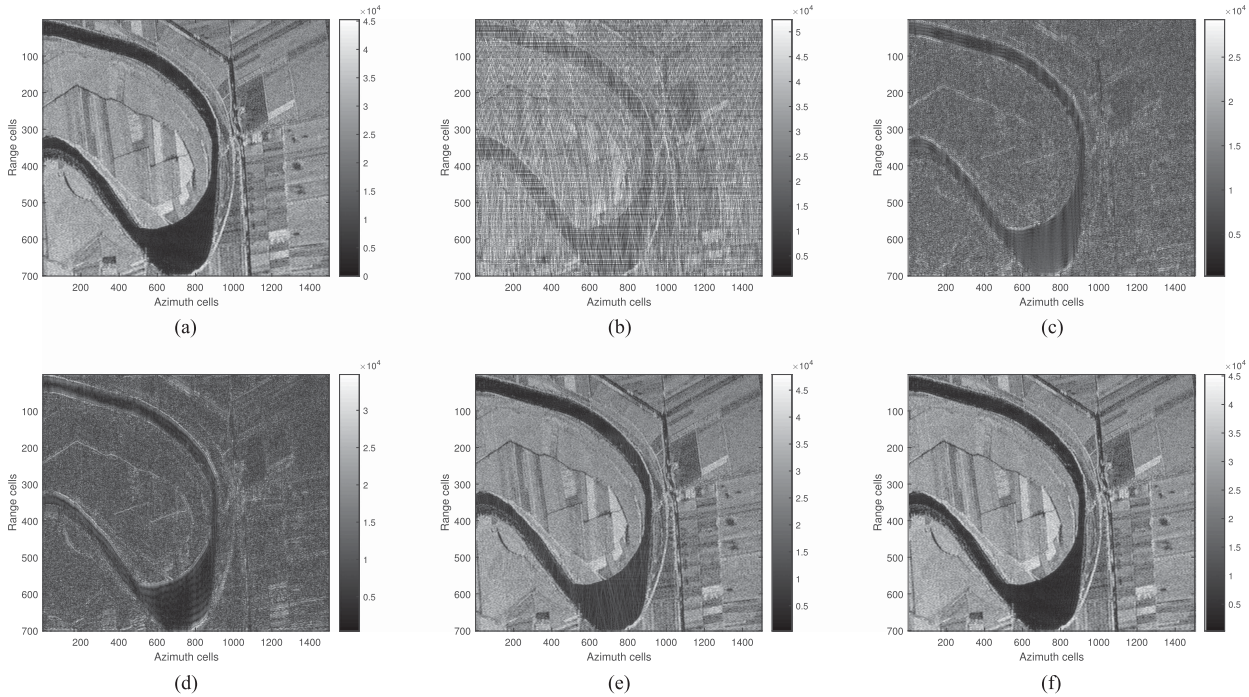

Fig. 8. Comparison of SAR images obtained by different RFI suppression methods. (a) Original SAR image without RFI. (b) SAR image polluted by RFIs. (c) RFI suppression by the FNF method. (d) RFI suppression by the IAA method. (e) RFI suppression by the SR method. (f) RFI suppression by the proposed SPC method.

SAR spectrum, greatly degrading the quality of the final SAR image. This is reflected in Fig. 8(c) that the ground information is destroyed, and no geometrical features of the scene appear. To a certain extent, the IAA method is similar to the FNF method, i.e., signal loss is unavoidable, but the former suppresses RFIs in the time–frequency domain by noting that RFIs are narrowband in each instant time slice, even RFIs are wideband. Therefore, relatively, losses of SAR signals are greatly reduced. We can see in Fig. 8(d) that some edge geometrical features of ground targets are preserved. Note that Fig. 8(b) and (c) seems dark compared to the other subfigures. Also, from the corresponding color bars of the two subfigures, we see that their energies are lower. This observation is consistent with the above analyses.

Quite different from the above two methods, the SR method aims at recovering SAR signals from the polluted SAR data to achieve an equivalent suppression effect, but not suppressing RFIs directly. Thus, we see that SR can greatly protect SAR signals from Fig. 8(e). Also, the SNR index of the SR method is 8.8916 dB, which is higher than the above two methods. Nevertheless, some energies of RFIs will also be recovered. In the river backgrounds in Fig. 8(e), one can still see some residual bright lines.

As the matter of fact, what these methods have in common, we see, is that they are facing the case that SAR signals and RFIs are overlapped in the frequency or time–frequency domain. Therefore, inevitably, either some SAR signals are suppressed or some RFIs are retained, both of which will degrade the SAR image quality. In general, RFIs and SAR signals are also overlapped in the Doppler domain since they have the same Doppler support area. In the proposed method, Doppler support areas of SAR signals are shifted through the proposed coding strategy. Therefore, in this case, RFIs and SAR signals are separated in the first place in the Doppler domain. Specifically, RFIs are in a certain Doppler bandwidth, while SAR signals are out of it. Thus, we can suppress RFIs, as well as protect SAR signals simultaneously. That is why the proposed method outperforms the others. Note that the SNR index of the proposed method is 16.5493 dB, which is higher than other methods, demonstrating the effectiveness of the proposed SPC method in RFI suppression.

B. DJ Suppression Performance Analyses

In this subsection, we will discuss the DJ suppression performance of the proposed method. Here, we choose the RPC [28] and the AQPC [29] methods as comparisons. To stay the integrality of the whole procedure of the proposed method, still we choose the parameters in Table I and the same detection scene in Fig. 8(a). Fig. 9 shows the experiment results.

By comparing Fig. 9(a) and (b), one can find that the false scene formed by DJs is greatly deceptive. On the other hand, intuitively, we see that in Fig. 9(d) and (f), the false scene disappears, while in Fig. 9(c) and (e), some energies of DJ still be retained. In this part, we still use RMSE and SNR as indices of quantitative experiments. Numerical experimental results are shown in Table III.

From Table III, one can see that the SNR index of the AQPC method is 51.1538 dB, which is the highest and means that the AQPC method outperforms the rest of methods, while the index of the proposed SPC-DBF2 method is 50.5422 dB, which is

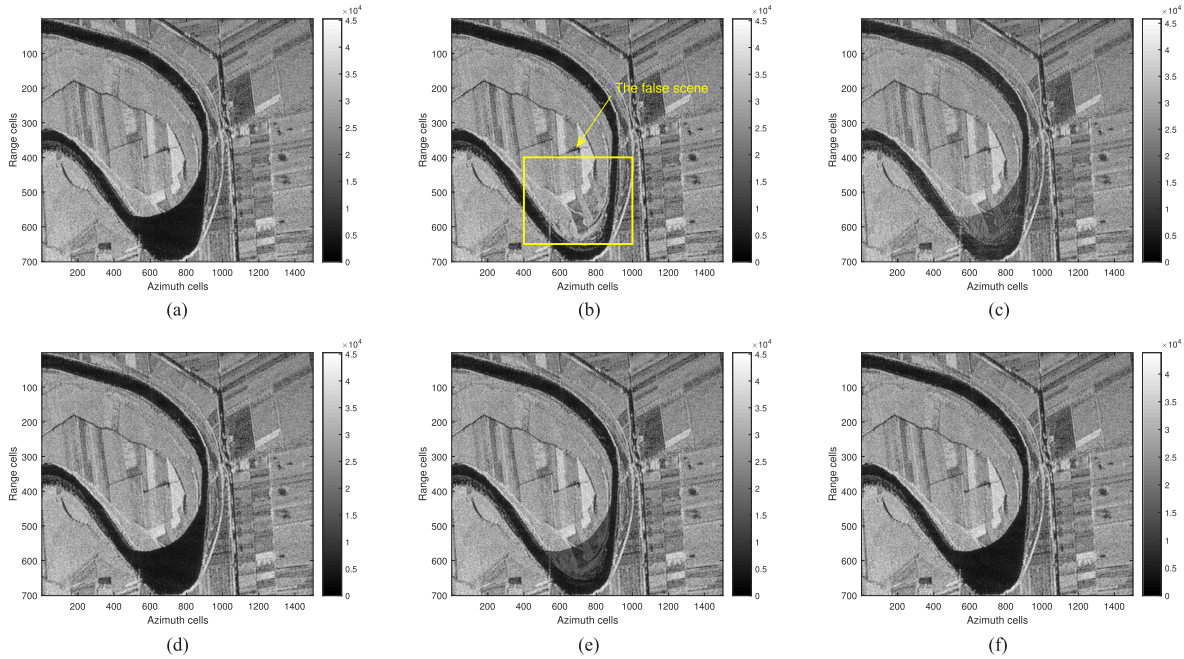

Fig. 9. Comparison of SAR images obtained by different DJ suppression methods. (a) Original SAR image without DJ. (b) SAR image polluted by DJ. (c) DJ suppression by the RPC method. (d) DJ suppression by the AQPC method. (e) DJ suppression by the proposed SPC-DBF1 method. (f) DJ suppression by the proposed SPC-DBF2 method.

TABLE III
QUANTITATIVE RESULTS OF DJ SUPPRESSION

Method	RMSE	SNR (dB)
RPC	17.7591	9.7119
AQPC	0.1504	51.1538
SPC-DBF1	1.6665	30.2641
SPC-DBF2	0.1614	50.5422

very close to the former, demonstrating the effectiveness of the proposed method in DJ suppression. Here, we make analyses about the above experiment results. Owing to the random coding strategy, in the RPC method, after the decoding procedure, DJs are with random Doppler centers. Although the false scene formed by DJs is not deceptive anymore, it still appears in the SAR image as a noise-like patch. This is shown in Fig. 10(a) that energies of DJs spread out into the whole Doppler domain, i.e., some of them enter into the Doppler bandwidth where SAR signals locate, even after Doppler filtering. Undoubtedly, these residual DJs impact the final SAR image result. For the AQPC method, through the quadratic-phase coding and decoding strategy, Doppler centers of DJs will be shifted by $f_{\mathrm{PRF}}/2$, while Doppler centers of SAR signals will not be shifted. Thus, under the same condition of inequality (18), Doppler histories of DJs and SAR signals are separated in the Doppler domain. This is also shown in Fig. 10(b). Therefore, after the Doppler filtering, one can obtain the cleaned SAR data.

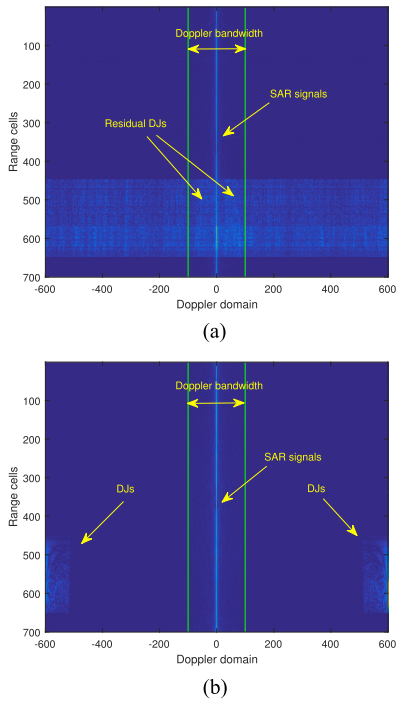

Fig. 10. Energy distributions of SAR signals and DJs in the range–Doppler domain. (a) RPC. (b) AQPC.

For the proposed SPC method, as discussed before, SPC-DBF1 can effectively enhance the SJR, but cannot greatly suppress DJs. It can be seen in Fig. 9(e) that the false scene still exists with deception, but its energy is low. On the contrary, SPC-DBF2 can suppress DJs greater. Nevertheless, SAR signals from each subpulse cannot achieve completely coherent accumulation at this time. Therefore, compared to the AQPC method, energies of SAR signals will be reduced slightly. That is why the value of the SNR index of SPC-DBF2 is a little less than the one of AQPC.

Remark: Although the AQPC method outperforms the proposed method in DJ suppression, it has no ability to suppress RFI. In fact, what the AQPC changes is the Doppler chirp rate, but not the Doppler support area. That is, the Doppler support area of SAR will not be shifted. Therefore, RFIs and SAR will not be separated in the Doppler domain. Readers are referred to [29] to see more details.

V. Conclusion

Previous works about interference suppression in SAR focus on a single kind of interference. In this article, we propose a joint RFI and DJ suppression method for single-channel SAR systems, which is a great advance. Specifically, the proposed SPC method effectively separates RFIs and SAR signals, having the ability to suppress RFIs as well as protect SAR signals. Also, SPC can suppress DJs by DBF technology with the designed weight vectors. Results of numerical experiments are provided to demonstrate the effectiveness of the proposed method.

Acknowledgment

The authors would like to thank all the anonymous reviewers and editors for their useful comments and suggestions that greatly improved this article.

References

[1] M. Tao, J. Su, Y. Huang, and L. Wang, "Mitigation of radio frequency interference in synthetic aperture radar data current status and future trends," *Remote Sens.*, vol. 11, pp. 2438–2462, 2019.

[2] N. Li, Z. Lv, and Z. Guo, "Observation and mitigation of mutual RFI between SAR satellites: A case study between chinese GaoFen-3 and European Sentinel-1A," *IEEE Trans. Geosci. Remote Sens.*, vol. 60, 2022, Art. no. 5112819.

[3] N. Li, H. Zhang, Z. Lv, L. Min, and Z. Guo, "Simultaneous screening and detection of RFI from massive SAR images: A case study on European Sentinel-1," *IEEE Trans. Geosci. Remote Sens.*, vol. 60, 2022, Art. no. 5231917.

[4] H. Yang, Y. He, Y. Du, T. Zhang, J. Yin, and J. Yang, "Two-dimensional spectral analysis filter for removal of LFM radar interference in space-borne SAR imagery," *IEEE Trans. Geosci. Remote Sens.*, vol. 60, 2022, Art. no. 5219016.

[5] F. Zhou, B. Zhao, M. Tao, X. Bai, B. Chen, and G. Sun, "A large scene deceptive jamming method for space-borne SAR," *IEEE Trans. Geosci. Remote Sens.*, vol. 51, no. 8, pp. 4486–4495, Aug. 2013.

[6] N. Li, Z. Lv, and Z. Guo, "Pulse RFI mitigation in synthetic aperture radar data via a three-step approach: Location, notch, and recovery," *IEEE Trans. Geosci. Remote Sens.*, vol. 60, 2022, Art. no. 5225617.

[7] T. Bollian, M. Younis, and G. Krieger, "On-ground RFI mitigation for spaceborne multichannel SAR systems using auxiliary beams," *IEEE Trans. Geosci. Remote Sens.*, vol. 60, 2022, Art. no. 5221918.

[8] F. Silva, E. Cetin, and W. Martins, "Radio frequency interference detection using nonnegative matrix factorization," *IEEE Trans. Aerosp. Electron. Syst.*, vol. 58, no. 2, pp. 868–878, Apr. 2022.

[9] S. Buckreuss and R. Horn, "E-SAR P-band SAR subsystem design and RF-interference suppression," in *Proc. IEEE Int. Geosci. Remote Sens. Symp.*, 1998, pp. 466–468.

[10] F. Meyer, J. Nicoll, and A. Doulgeris, "Correction and characterization of radio frequency interference signatures in L-band synthetic aperture radar data," *IEEE Trans. Geosci. Remote Sens.*, vol. 51, no. 10, pp. 4961–4972, Oct. 2013.

[11] W. Xu et al., "RFI suppression for SAR systems based on removed spectrum iterative adaptive approach," *Remote Sens.*, vol. 12, pp. 3520–3544, Oct. 2020.

[12] Z. Liu, G. Liao, and Z. Yang, "Time variant RFI suppression for SAR using iterative adaptive approach," *IEEE Geosci. Remote Sens. Lett.*, vol. 10, no. 6, pp. 1424–1428, Nov. 2013.

[13] Z. Yang, W. Du, Z. Liu, and G. Liao, "WBI suppression for SAR using iterative adaptive method," *IEEE J. Sel. Topics Appl. Earth Observ. Remote Sens.*, vol. 9, no. 3, pp. 1008–1014, Mar. 2016.

[14] F. Zhou, M. Xing, X. Bai, G. Sun, and Z. Bao, "Narrow-band interference suppression for SAR based on complex empirical mode decomposition," *IEEE Geosci. Remote Sens. Lett.*, vol. 6, no. 3, pp. 423–427, Jul. 2009.

[15] M. Tao, F. Zhou, J. Liu, Y. Liu, Z. Zhang, and Z. Bao, "Narrow-band interference mitigation for SAR using independent subspace analysis," *IEEE Trans. Geosci. Remote Sens.*, vol. 52, no. 9, pp. 5289–5301, Sep. 2014.

[16] H. Yang, C. Chen, S. Chen, F. Xi, and Z. Liu, "A dictionary-based SAR RFI suppression method via robust PCA and chirp scaling algorithm," *IEEE Geosci. Remote Sens. Lett.*, vol. 18, no. 7, pp. 1229–1233, Jul. 2021.

[17] X. Lu, J. Yang, W. Yu, W. Su, H. Gu, and T. S. Yeo, "Enhanced LRR-based RFI suppression for SAR imaging using the common sparsity of range profiles for accurate signal recovery," *IEEE Trans. Geosci. Remote Sens.*, vol. 59, no. 2, pp. 1302–1318, Feb. 2021.

[18] H. Liu, D. Li, Y. Zhou, and T.-K. Truong, "Joint wideband interference suppression and SAR signal recovery based on sparse representations," *IEEE Geosci. Remote Sens. Lett.*, vol. 14, no. 9, pp. 1542–1546, Sep. 2017.

[19] G. Nie, G. Liao, and C. Zeng, "NBI suppression method for SAR based on sparse segmentation search," *IEEE Geosci. Remote Sens. Lett.*, vol. 19, 2022, Art. no. 4510805.

[20] Y. Huang, Z. Chen, C. Wen, J. Li, X.-G. Xia, and W. Hong, "An efficient radio frequency interference mitigation algorithm in real synthetic aperture radar data," *IEEE Trans. Geosci. Remote Sens.*, vol. 60, 2022, Art. no. 5224912.

[21] Y. Huang et al., "HRWS SAR narrowband interference mitigation using low-rank recovery and image-domain sparse regularization," *IEEE Trans. Geosci. Remote Sens.*, vol. 60, 2022, Art. no. 5217914.

[22] H. Liu, D. Li, Y. Zhou, and T.-K. Truong, "Simultaneous radio frequency and wideband interference suppression in SAR signals via sparsity exploitation in time–frequency domain," *IEEE Trans. Geosci. Remote Sens.*, vol. 56, no. 10, pp. 5780–5793, Oct. 2018.

[23] L. Nguyen and T. Tran, "Efficient and robust RFI extraction via sparse recovery," *IEEE J. Sel. Topics Appl. Earth Observ. Remote Sens.*, vol. 9, no. 6, pp. 2104–2117, Jun. 2016.

[24] X. Lu, Y. Zhao, J. Yang, W. Su, H. Gu, and T. S. Yeo, "An efficient method for single-channel SAR target reconstruction under severe deceptive jamming," *IEEE Geosci. Remote Sens. Lett.*, vol. 17, no. 2, pp. 237–241, Feb. 2020.

[25] B. Zhao, L. Huang, and J. Zhang, "Single channel SAR deception jamming suppression via dynamic aperture processing," *IEEE Sens. J.*, vol. 17, no. 13, pp. 4225–4230, Jul. 2017.

[26] S. Liu, B. Zhao, L. Huang, B. Li, Y. Wu, and W. Bao, "Target reconstruction against deceptive jamming for single-channel SAR: An imagery domain approach," *IEEE Geosci. Remote Sens. Lett.*, vol. 19, 2022, Art. no. 4505205.

[27] B. Zhao, L. Huang, J. Li, and P. Zhang, "Target reconstruction from deceptively jammed single-channel SAR," *IEEE Trans. Geosci. Remote Sens.*, vol. 56, no. 1, pp. 152–167, Jan. 2018.

[28] Q. Feng, H. Xu, Z. Wu, and B. Sun, "Deceptive jamming suppression for SAR based on time-varying initial phase," in *Proc. IEEE Int. Geosci. Remote Sens. Symp.*, 2016, pp. 4996–4999.

[29] Z. Tang, Y. Deng, H. Zheng, and R. Wang, "High-fidelity SAR intermittent sampling deceptive jamming suppression using azimuth phase coding," *IEEE Geosci. Remote Sens. Lett.*, vol. 18, no. 3, pp. 489–493, Mar. 2021.

[30] Y. Huang, G. Liao, Z. Zhang, Y. Xiang, J. Li, and A. Nehorai, "Fast narrowband RFI suppression algorithms for SAR systems via matrix-factorization techniques," *IEEE Trans. Geosci. Remote Sens.*, vol. 57, no. 1, pp. 250–262, Jan. 2019.

Guoli Nie was born in Hunan, China, in 1996. He received the B.S. degree in electronic engineering in 2018 from Xidian University, Xi'an, China, where he is currently working toward the Ph.D. degree in signal and information processing with the National Laboratory of Radar Signal Processing.

His research interests include radio frequency interference and deceptive jamming suppression in synthetic aperture radar.

Guisheng Liao (Senior Member, IEEE) was born in Guilin, China, in 1963. He received the B.S. degree in mathematics from Guangxi University, Nanning, China, in 1985, and the M.S. degree in computer science and the Ph.D. degree in electrical engineering from Xidian University, Xi'an, China, in 1990 and 1992, respectively.

He is currently a Yangtze River Scholars Distinguished Professor with the National Laboratory of Radar Signal Processing, Xidian University, where he is also the Dean of the Hangzhou Institute of Technology. Since 2009, he has been the Evaluation Expert for the International Cooperation Project of Ministry of Science and Technology in China. Since 2007, he has been the lead of Yangtze River Scholars Innovative Team and devoted in advanced techniques in signal and information processing. Since 2006, he has been the Panelists for the medium and long term development plan in high resolution and remote sensing systems. From 1999 to 2000, he was a Senior Visiting Scholar with the Chinese University of Hong Kong, Hong Kong. His research interests include array signal processing, space-time adaptive processing, radar waveform design, and airborne/space surveillance and warning radar systems.

Cao Zeng (Member, IEEE) was born in Hubei, China, in 1979. He received the B.E. degree in electronic engineering, the M.S. and Ph.D. degrees in signal and information engineering from Xidian University, Xi'an, China, in 2001, 2004, and 2008, respectively.

He is currently a "Hua Mountain" Professor with Xidian University. His research interests include array signal processing, moving target detection, and multisource information fusion.

Xuepan Zhang was born in Hebei, China. He received the B.S. and Ph.D. degrees in electrical engineering from Xidian University, Xi'an, China, in 2010 and 2015, respectively.

He is currently a Professor with the Hangzhou Institute of Technology, Xidian University. His research interests include synthetic aperture radar, ground moving target indication, and radio frequency interference analysis and suppression.

Dongchen Li received the B.E. and Ph.D. degrees in electrical engineering from Xidian University, Xi'an, China, in 2010 and 2016, respectively.

He is currently a Senior Engineer with the CSSC Systems Engineering Research Institute, Beijing, China. His current research interests include target detection, data mining, and drone mission information processing.